

1 **A rapid unravelling of mycobacterial activity and of their susceptibility to antibiotics**

2

3 A. Mustazzolu¹⁺, L. Venturelli²⁺, S. Dinarelli³, K. Brown⁴, R.A. Floto⁴, G. Dietler², L. Fattorini¹,
4 S. Kasas², M. Girasole³ and G. Longo^{3#}

5 + These authors contributed equally to the work

6 ¹ Istituto Superiore di Sanità, Rome, IT

7 ² LPMV - IPHYS, Ecole Polytechnique Fédérale Lausanne, Lausanne, CH

8 ³ Istituto di Struttura della Materia, Consiglio Nazionale delle Ricerche, Rome, IT

9 ⁴ Molecular Immunity Unit, University of Cambridge, Cambridge, UK

10 # All materials and correspondence must be addressed to Giovanni Longo, Istituto di Struttura della
11 Materia – CNR, Via del Fosso del Cavaliere 100, 00133 Roma, Italy. Email: longo@ism.cnr.it; Tel.
12 +39 06 45488 299

13

14 **Running title:** Fast analysis of mycobacteria and their susceptibility

15

16 **Keywords:** mycobacteria; susceptibility; nanomotion sensor; fast characterization; antibiotic
17 response; collective movements; metabolic activity

18 **Abstract**

19 The development of antibiotic-resistant bacteria is a worldwide health-related emergency that calls
20 for new tools to study the bacterial metabolism and to obtain fast diagnoses. Indeed, the
21 conventional analysis timescale is too long and affects our ability to fight infections. Slowly
22 growing bacteria represent a bigger challenge, since their analysis may require up to months.
23 Among these bacteria, *Mycobacterium tuberculosis*, the causative agent of tuberculosis has caused,
24 only in 2016 more than 10 million new cases and 1.7 million deaths. We employed a particularly
25 powerful nanomechanical oscillator, the nanomotion sensor, to characterize rapidly and in real time
26 a tuberculous and a non-tuberculous bacterial species, *Bacillus Calmette-Guérin* and
27 *Mycobacterium abscessus* exposed to different antibiotics.

28 Here, we show how high speed and high sensitivity detectors, the nanomotion sensors, can provide
29 a rapid and reliable analysis of different mycobacterial species, obtaining qualitative and
30 quantitative information on their response to different drugs.

31 This is the first application of the technique to tackle the urgent medical issue of mycobacterial
32 infections, evaluating the dynamic response of bacteria to different antimicrobial families and the
33 role of the replication rate in the resulting nanomotion pattern. In addition to a fast analysis, which
34 could massively benefit patients and the overall healthcare system, we investigated the real-time
35 response of the bacteria to extract unique information on the bacterial mechanisms triggered in
36 response to the antibacterial pressure, with consequences both at the clinical and at the
37 microbiological level.

38

39

40

41 Introduction

42 Providing fast and reliable antibiotic susceptibility data, which allows initiating prompt and
43 appropriate therapy schedules, is a main task of the clinical laboratory. While molecular techniques
44 (*i.e.* MALDI-TOF Mass Spectrometry (MS) or PCR-based gene amplification)(1, 2) have radically
45 changed the time-frame for Gram positive (+) and negative (-) bacterial identification (ID), most of
46 current methods for antimicrobial susceptibility testing (AST) are still based on fluorescence
47 staining or phenotypic assays(1, 3) which may require days, or even weeks, depending on the
48 bacterial species. In conventional clinical workflow, the sample (*e.g.* blood, spinal fluid, urine,
49 feces, nasal or throat swabs) is harvested from patients, streaked on agar nutrient media and, after
50 12-24 hours incubation, transferred for further analysis. This unavoidable culture step results in
51 isolation of microorganisms in liquid cultures containing up to $10^8 - 10^9$ Colony Forming Units
52 (CFU)/ml.(4) ID and culture-based AST are performed after this incubation time, and can last more
53 than 24 hours.(5) Similar protocols are commonly used for slowly growing bacteria such as
54 mycobacteria but, in these cases, the incubation time can be longer than a week (*e.g.* in the MGIT
55 960 system), and more than one month may be required to obtain ID and AST.(5) This long
56 timeframe, under the pressure of life-threatening infections, often results in imprudent use or misuse
57 of antibiotics. Early appropriate therapy will significantly reduce the spread of pathogenic bacteria
58 into the population. This will lead to higher patient survival rate, lower distress and an optimized
59 use of the limited resources of healthcare systems.(6, 7)

60 Many options are emerging to achieve a rapid, accurate and cost-effective pathogen characterization
61 of bacterial response to drugs, ranging from molecular to rapid phenotypic techniques to plasmonic
62 single cell assays.(8-11) The conventional AST molecular techniques rely mainly on the
63 determination of the genetic fingerprint associated with resistance to a specific antibiotic, including
64 real-time PCR (RT PCR), DNA microarrays, Next-generation sequencing (NGS), cell lysis-based
65 approaches, whole-genome sequencing, and MALDI-TOF MS.(12-16) Even though the

66 aforementioned techniques can provide fast and high-throughput results, they still present profound
67 drawbacks. For instance, their outcome is strongly dependent on specific drug-target genes, which
68 can only be indicative of the actual antibiotic resistance, leaving a large gap for drug phenotypic
69 response.

70 Novel single-cell techniques are have gained importance in the last decade in particular for cancer-
71 related applications. Nevertheless, the analysis of bacterial susceptibility requires the concurrent
72 evaluation of hundreds or thousands of bacteria to assess response at the population level. Thus,
73 their application is mostly limited to the research laboratory and their low throughput hinders their
74 transition to a clinical susceptibility test.

75 Most commercial phenotypic assays rely on bacterial replication to deliver a correct AST and the
76 timescale for antibiogram determination may range from days, for rapidly replicating bacteria, to
77 weeks or months, for slowly growing and fastidious germs. To shorten turnaround times and costs,
78 several automated systems are now available, including, for instance, MicroScan WalkAway
79 (Beckman Coulter), BD Phoenix (Dickinson Becton), Vitek-2 (bioMérieux), SIDECAR
80 (Alifax).(17, 18) The outcome is a relatively rapid susceptible/resistant response, which is available
81 to the clinician as soon as the second day from the first examination of the sample, with large
82 advantages for treatment, but still too long for severe infections (*e.g.* meningitis, sepsis). (1, 3) In
83 addition, most of these techniques provide no clue on the particular drug effect or on the counter
84 mechanisms employed by bacteria to react to antibiotic compounds.

85 Among the alternatives to conventional microbiological assays, small and extremely sensitive
86 nanomechanical oscillators(19) stand out as very promising candidates(8, 9, 20, 21). At first, such
87 devices were employed in Atomic Force Microscopes (AFM) to study dynamic behaviour in
88 cells(22) or proteins.(23, 24) Nowadays they are increasingly used for the detection of very small
89 masses(25) or for nano-stress sensing in molecular biology(26) and their sensitivity and versatility

90 is exploited in lab-on-a-chip devices to measure bio-molecular interactions(27) or mass
91 variations in biological systems, including bacteria.(28, 29) Two major factors limit most of the
92 available nanomechanical systems: (i) they require air or vacuum conditions for the measurements;
93 (ii) they need bacteria to replicate directly on the sensors, to determine cell viability through mass
94 change or local stress alterations. This reflects on the time required to perform analysis, and on the
95 range of information that can be obtained, based on life or death assessments.

96 Very recently, we have introduced a new way of exploiting the capabilities of cantilever
97 nanosensors: the nanomotion sensor (NMS)(30, 31). By exploiting the intimate link between life
98 and motion, measuring the fluctuations of flexible cantilevers that act as solid support for
99 microorganisms, we can monitor in real time the metabolism of living organisms.(32) The sensor's
100 fluctuations strongly depend on the microorganisms' metabolic activities, which combine energy
101 consumption, cell vibration and movement. The sensitivity of the technique allows detecting the
102 energy consumption of few ATP molecules, as demonstrated in previous works using Finite
103 Elements Modelling or studying conformational changes in quaternary protein structures. (31, 33)
104 Thus, the NMS can be used to evaluate the fluctuations of a very limited number of viable
105 specimens (single mammalian cells or tens of bacteria).(32, 34-37)

106 By measuring the fluctuations as a function of time and of external conditions, the NMS delivers a
107 unique insight on microorganisms response to environmental, chemical or physical stimuli.(32) The
108 amplitude and the low frequency of these fluctuations (<1 kHz) help circumventing the major
109 limitations of current nanomechanical sensors: the NMS can be used under various conditions (*i.e.*
110 buffer solutions or growing media), and the viable specimens are attached on both sides of the
111 sensor, reducing complexity and cost of each experiment. In addition, due to the time resolution of
112 the NMS, these experiments allow investigating in real-time and with sensitivity in the Angstrom-
113 to-micron range(33) the evolving metabolism of the adsorbed bacteria, long before a single
114 replication(30, 31), suggesting that the analysis timescales are only marginally dependent on

115 bacterial duplication rates, as demonstrated by studying *B. pertussis*, which replicates in 48 hours
116 (38). In addition, the sensitivity of these sensors allows extracting a measurable signal from groups
117 of less than 100 bacterial cells, leading to a drastic reduction of incubation times. Overall, the
118 outcome is a quantitative evaluation of the real bacterial response to the applied stimuli, on a time-
119 scale (hours) comparable to the fastest molecular analyses.(39) Furthermore, the real-time
120 monitoring of a nanomotion susceptibility test (N-AST) reveals a different kind of information on
121 the bacterial behaviour compared to conventional phenotypic and genetic studies, with the potential
122 to improve therapeutic interventions, which are paramount for clinical decisions and, hopefully,
123 therapeutic outcomes, as demonstrated in previous works on rapidly growing bacteria.(40) For this
124 reason, coupling the NMS with other conventional techniques could help to better unravel which
125 molecular processes arise to account for specific observed motion-change behaviour.

126

127 **Results**

128 We exploited the capabilities of the NMS to study slowly growing *Mycobacterium bovis* bacillus
129 Calmette-Guérin (BCG) and the fast growing nontuberculous mycobacterium (NTM)
130 *Mycobacterium abscessus*.(41) In particular, the former species belongs to the *M. tuberculosis*
131 complex (MTC), which includes *M. tuberculosis* (Mtb), *M. africanum*, representing a growing
132 medical emergency in both developing and developed regions.(42) By studying their nanomotion,
133 we characterized the interaction between these two species and three antibacterial drugs, and were
134 able to determine in a matter of hours their susceptibility, calculating their minimum inhibitory
135 concentration (MIC) and minimum bactericidal concentrations (MBC). Furthermore, we exploited
136 the real-time analysis of the NMS to evaluate the peculiar responses of these bacteria to the
137 different antibacterial agents. We chose to work with a relatively large number of bacteria on the
138 sensor (approximately between 100 and 1000 cells) to ensure a good population-level analysis of

139 the susceptibility and to average out the possible presence of outliers or single naturally resistant
140 microorganisms.

141 In preliminary experiments, we determined whether NMS preparation protocols influenced the
142 viability of BCG and *M. abscessus* in the MGIT medium. Overall, we kept the bacteria for at least
143 200 min in the analysis chamber by monitoring the oscillations over time. As shown in Figure 1, the
144 variance of the nanomotion signals remained constant over time, indicating that the bacteria were
145 viable for the entire control experiment.

146 **BCG**

147 We performed a series of experiments involving exposure of BCG to RIF or INH, two first line
148 anti-TB drugs inhibiting the DNA-dependent RNA polymerase, and specific enzymes implicated in
149 cell wall synthesis, respectively.(42, 43) We selected this species because it belongs to the MTC, is
150 not dangerous for humans, and can be safely handled in a Biosafety Level 2 laboratory, constituting
151 a safe NMS testing ground for the study of more dangerous mycobacteria, including *Mtb*.

152 When exposed to bactericidal doses of these agents, the BCG produced a sharp reduction of the
153 sensor's fluctuations, underlining the drug's activity. In a typical experiment, the outcome of the
154 exposure to a bactericidal dose of INH (2 $\mu\text{g/ml}$) could be determined in less than 30 min (Figure
155 2). On the other hand, after exposure to a high dose of RIF (0.7 $\mu\text{g/ml}$ in Figure 3), we observed a
156 reduction in the sensor's movement, demonstrating a slower bactericidal effect and confirming
157 bacterial death which required almost 2 hours.

158 The subsequent step in the analysis of the response of BCG to these antibacterial agents consisted in
159 a series of dose-dependence experiments. The results, summarized in Figure 4a for INH and 4b for
160 RIF, indicate for each experiment the relative reduction of the nanomotion fluctuations. In both
161 cases, the linear fit of the sigmoid curve was used to determine the MIC and MBC values. The

162 obtained values were MIC 0.09 ± 0.03 $\mu\text{g/ml}$ and MBC 0.17 ± 0.03 $\mu\text{g/ml}$ for INH; MIC 0.15 ± 0.07
163 $\mu\text{g/ml}$ and MBC 0.4 ± 0.07 $\mu\text{g/ml}$ for RIF. The MICs of BCG Pasteur determined by NMS differed
164 by about 1-fold dilution from those determined by conventional proportion methods (0.2 *versus*
165 0.09 $\mu\text{g/ml}$ for INH, and 0.063 *versus* 0.15 $\mu\text{g/ml}$ for RIF, respectively).(44-46) Such discrepancy
166 between the conventionally measured MIC and the N-AST is something that has been also
167 highlighted in previous experiments involving rapidly growing bacteria.(31, 39) This difference can
168 be interpreted by invoking many factors, such as growth conditions, measurement geometry or
169 temperature. It must be noted that conventional and NMS assays monitor different metabolic
170 parameters. In most conventional analyses, the MIC is identified by the bacterial ability to replicate,
171 while for the NMS, this concentration is associated to the reduction of the sensor's fluctuations
172 associated to alterations in the bacterial membrane elasticity(36, 37) or to their internal metabolic
173 activity. Indeed, while the information content is the similar, the concentration at which one or the
174 other phenomenon occurs can be different.

175 In addition to these quantitative susceptibility results, performing a real-time analysis on antibiotics
176 susceptibility allowed us to evaluate how the drug pressure influenced the investigated
177 microorganisms, including their peculiar response patterns and typical timescales. For instance,
178 INH exposure, even if using sub-MIC concentrations, caused an immediate response of BCG,
179 which was registered as a fluctuation intensity increase that lasted 10-15 min before a rapid decay
180 of the movements. After few tens of minutes, if the concentration was not bactericidal (*i.e.* 0.025
181 $\mu\text{g/ml}$ in Figure 5a), the variance of the fluctuations recovered their intensity and, returned to values
182 comparable to those measured before the antibiotic injection. This entire response pattern did not
183 last more than 20 minutes. On the other hand, if the drug concentration was higher than the MBC
184 (*e.g.* 1 $\mu\text{g/ml}$, Figure 6), the response was more complex. After an initial rise of the oscillations, the
185 movements rapidly decreased to lower values for up to 25 min, followed by few seconds of wide
186 fluctuations. This biphasic pattern repeated itself several times for more than 1 h, until the

187 fluctuations stabilized to low values, indicating the death of the BCG. A possible interpretation of
188 this pattern is related to BCG clumping: these bacteria exploit their waxy coating to form cell
189 aggregates not completely dissolved during sample preparation procedures. In such clumps,
190 external bacteria are expected to be metabolically more active than internal ones, partially shielding
191 them from some environmental attacks. In this view, the bactericidal antibiotics could kill, at first,
192 the cells of the external layer, and then the internal bacteria would be activated, resulting in the
193 movement-stasis pattern we observed and measured. Clumping is an already known defense
194 mechanism in microbiology and can be found in many different species, such as *Candida albicans*,
195 or in self-aggregation in *Escherichia coli* or in flocculation in *Saccharomyces cerevisiae* (47-50) but
196 it has never been reported in this way for BCG.

197 While we identified these peculiar movements in INH-exposed BCG, these were never seen in RIF
198 experiments (Figure 5b), suggesting that this behavior is strictly dependent on the response
199 mechanism of BCG to INH. Indeed, the response against 0.07 $\mu\text{g/ml}$ of RIF did not involve a strong
200 initial reaction to the drug, with fluctuations lasting from 1 to 2 h. In some cases, after minutes from
201 drug exposure, we measured a temporary reduction of movements, which lasted up to 30 min,
202 followed by full recovery of the nanomotion fluctuations. Furthermore, in RIF-exposed BCG, we
203 never identified the oscillating patterns seen for INH. A possible interpretation of the different
204 reported behavior respect to the two different drugs could rely on their different time-scale of the
205 effect. While INH affects the cell wall synthesis, its effect is quite fast and the shielding of the
206 clumping could produce a visible transitional oscillation. On the other hand, since RIF targets RNA
207 polymerase consequently blocking protein translation, its longer timescale could cover the
208 aforementioned effect.

209 ***M. abscessus***

210 To investigate the response of drugs against *M. abscessus*, we used the protein synthesis inhibitor,
211 amikacin (AK), because this organism is known to be resistant to INH and RIF. In the presence of a
212 bactericidal concentration of the drug (10 $\mu\text{g/ml}$ in Figure 7a), *M. abscessus* did not show an
213 immediate response, without alterations of the fluctuations for the first 30 min, followed by a sharp
214 decrease of the movements between 50 and 70 minutes, after which the fluctuations did not recover.
215 When non-bactericidal doses were used (1 $\mu\text{g/ml}$ in Figure 7b), a lag phase of approximately 10-25
216 min was observed, followed by a full recovery of the nanomotion signal. This trend is in line with
217 the NMS response of *Staphylococcus aureus* exposed to cefoxitin(31) or *E. coli* to ceftriaxone(39).
218 It is worth noting that the response time of *M. abscessus* to AK (50-70 minutes) is longer than in the
219 BCG-INH case (20-30 min) and comparable with the BCG-RIF timescales (80-100 min). This can
220 be attributed to the different mechanisms of action of AK compared to INH. Indeed, INH inhibits
221 the cell wall synthesis and is expected to have a more rapid effect than RIF and AK, which inhibit
222 the protein synthesis. Remarkably, the response times of the BCG and *M. abscessus* are similar to
223 the typical timescales of the experiments involving rapidly replicating bacteria (between 15 and 60
224 minutes for both *E. coli* and *S. aureus*(31, 39)). This clearly demonstrates the nanomotion sensor's
225 independence to the replication rate of the specimens under investigation. Furthermore, it also
226 depicts the range of interesting new information that the technique can provide.

227 As done for BCG, we performed a series of dose-dependence measurements, in order to obtain
228 quantitative susceptibility results for *M. abscessus* exposed to AK (Figure 4c). The linear fit for the
229 sigmoid curve indicated a MIC of $1.7 \pm 0.6 \mu\text{g/ml}$ and a MBC of $7.8 \pm 0.6 \mu\text{g/ml}$. These
230 concentrations are in good agreement (within one dilution) with those present in literature for this
231 reference *M. abscessus* strain (3.1 versus 1.7 $\mu\text{g/ml}$).(51, 52)

232

233 **Discussion**

234 *M. tuberculosis* and NTM are the causative agents of extremely dangerous infections, such as TB,
235 which caused in 2016 more than 10.4 million new cases and 1.7 million deaths in developing and
236 industrialized countries (WHO Global TB Report 2017). A fast diagnosis of these bacteria will
237 allow a more specific, tailored treatment, more effective, better tolerated by the patient, and less
238 likely to produce relapses. An early diagnosis of infections from slowly growing bacteria could be
239 lifesaving and could significantly reduce the spread of harmful pathogens into the population,
240 leading to higher survival rate, lower distress and an improved use of the limited resources of the
241 healthcare system.(53, 54)

242 This work shows how the NMS can be used to obtain a rapid and reliable investigation of the MTC
243 and NTM, with possible impact in the early clinical and diagnostics fields. Indeed, while the clinical
244 application of the NMS has already been demonstrated on *E. coli*,(39) its importance to the study of
245 slowly growing germs can be safely suggested. In addition, the speed of the nanomotion analyses
246 can allow a rapid screening of innovative molecules and antitubercular agents, to accelerate and
247 reduce the costs for drug discovery and drug development.(55, 56) Furthermore, the NMS can
248 highlight the specific behavior of slowly growing bacteria during antibiotic treatment, evidencing
249 cooperative vibrations and activity reduction, which could not be determined using other
250 phenotypic techniques. This provides a better overview of the metabolism of slowly growing
251 bacteria in models more closely mimicking *in vivo* microenvironments and of their dynamic
252 responses to external stimuli, which is of great importance in medical and pharmacological TB
253 research. These results illustrate how N-AST can become a reliable and rapid investigation tool for
254 slowly growing bacterial species, providing also a new insight into the behavior of these bacteria
255 during antibiotic treatment.

256 The possibility to combine NMS and molecular biology assays would deliver a thorough
257 comprehension of the bacterial resistance mechanisms, which could provide invaluable information

258 to produce newer, more targeted drugs and anti-mycobacterial agents, to fight some of the deadlier
259 diseases of our times.

260

261 **Materials and methods**

262 **Substrates, enzymes and reagents**

263 Chemicals, phosphate buffered saline (PBS), glutaraldehyde and antibiotics rifampicin (RIF),
264 isoniazid (INH) and amikacin (AK), all with analytical grade, were obtained from Sigma-Aldrich
265 (St Louis, MO). MGIT 960 (MGIT) tubes (Becton-Dickinson Microbiology Systems, Sparks, MD)
266 were used to obtain the bacterial culture medium.

267

268 **Bacterial preparation and isolation**

269 *Mycobacterium bovis* BCG [American Type Culture Collection (ATCC) 27291 (Pasteur strain)]
270 cells, frozen at -70°C , were thawed, and grown in Löwenstein Jensen slants at 37°C for 3 weeks.
271 Few colonies were transferred in tubes containing 500 μl of MGIT medium. Since the BCG tends to
272 form clumps that are difficult to disaggregate, before transferring the bacteria-rich medium to the
273 nanomotion experiments we vortexed the tubes to ensure that any large bacterial clump was
274 dissolved or reduced. Still, as shown in Figure 8, small BCG clumps were present on the sensors.
275 The MIC of BCG Pasteur was determined using the proportion method. The characterizations
276 showed that, in good agreement with the values present in literature, the MICs were 0.2 $\mu\text{g}/\text{ml}$ for
277 INH(45) and 0.063 $\mu\text{g}/\text{ml}$ for RIF(46), respectively, with an uncertainty of one dilution.

278 *Mycobacterium abscessus* [ATCC 19977] cells frozen at -70°C were thawed, and the specimens
279 were grown in MGIT medium at 37°C for 3 days under continuous agitation. 1 ml of the bacteria-

280 rich medium was centrifuged (5000 rpm for 5 min), the pellet was re-suspended in PBS and
281 transferred directly to nanomotion experiments. The susceptibility values present in literature for
282 ATCC 19977 towards amikacin detail a MIC of 3.1 $\mu\text{g/ml}$, with an uncertainty of one dilution.(52)

283

284 **Nanomotion experiments**

285 The nanoscale movements of the microorganisms induced dynamic deflections of the NMS, which
286 we monitored in real-time, using the laser-based signal transduction typically used in most AFMs.
287 We collected these fluctuations in a time-dependent chart of the vertical movements of the sensor,
288 which appeared as a coloured noise signal, superposition of a large number of vibrations.. Overall, a
289 typical experiment lasted more than 2 hours divided in data chunks of at least 30 minutes. The
290 control experiments were carried out for at least 4 hours. In each experiment, the sensors were
291 followed in real-time using optical cameras.

292 We used a commercial Nanowizard III microscope (JPK Instruments, Berlin, DE) and custom
293 homemade devices developed in the Laboratories of Living Matter Physics at the EPFL (LPMV-
294 EPFL). The sensors chosen for the JPK experiments were the ONP-10 tipless AFM cantilevers from
295 Bruker (Bruker Nano Inc., MA, USA). For the homemade devices, we employed the SD-qp-CONT
296 tipless cantilevers (Nano and More GmbH, DE). For all experiments, we used sensors with spring
297 constant in the range of 0.08+-0.03 N/m, which demonstrated a good sensitivity coupled with
298 geometrical properties that ensured space for an adequate number of bacteria (as controlled through
299 optical images throughout each experiment). The data from the Nanowizard III microscope were
300 collected using the JPK software using a 10 kHz acquisition rate, while the data from the
301 experiments on the custom devices were collected using a USB-4431 DAQ card (National
302 Instruments, USA), using a 20 kHz acquisition rate. Remarkably, as a demonstration of the solidity

303 of the analysis technique, we were able to compare the results obtained with the two different
304 instrumentations, which exhibited similar sensitivity and noise levels.

305 To enhance bacterial adhesion, as established and detailed in many previous works, we chemically
306 treated the sensors. In literature, there are examples of fibronectin, poly-lysine, polyethylene imine,
307 APTES, glutaraldehyde, concanavalin or even collagen used for this purpose.(15, 40, 57-60) In
308 comparison with the specimens analyzed in some previous works,(61) the thick, hydrophobic and
309 waxy cell walls of mycobacteria required new immobilization strategies and the use of specific
310 culture media and drugs. In the present work, we exposed the sensors to 0.5% glutaraldehyde for
311 15 min, followed by rinsing in ultrapure water and air-drying. This immobilization protocol allowed
312 mycobacteria to adhere on the sensors with little influence on their metabolic activity (as
313 demonstrated by the control experiments depicted in Figure 1)

314 We equipped both instruments with closed custom analysis chambers, made of plastic or
315 polydimethylsiloxane (PDMS), which allowed performing experiments in liquid while changing the
316 medium with very low noise(62).

317 For the subsequent immobilization of the living bacteria on the sensors, we strictly followed a
318 protocol that ensured a remarkable adhesion of the cells on the sensors. Since the growth media
319 often contain complex molecules that could passivate the chemical functionalization on the sensor,
320 we washed twice in PBS an aliquot of MGIT-containing bacteria (by centrifuging cells at 3000xg
321 for 5 min, and re-suspending the pellet in 100 μ l of PBS with a final OD that ranged from 10^6 to 10^8
322 CFU). In order to let the bacteria adhere on the sensor we deposited a droplet (typically 20 μ l) of
323 the bacteria-rich PBS on the sensor and incubated at room temperature for about 15 min. This
324 protocol allows the formation of a roughly uniform distribution of bacteria on the sensor surface,
325 with an innate variability in their number and spatial distribution. Thereafter, we mounted the
326 sensor on the holder and inserted it into the analysis chamber, carrying 2 ml of MGIT medium for

327 the analyses. As shown in the optical images of the sensors during the experiments (Figure 8), an
328 approximate estimate of 100 to 1000 cells adhered to the NMS, while more complex procedures
329 must be carried out to obtain a quantitative determination.(31) It is worth highlighting that the
330 immobilization protocol produces a variability in the absolute value of the oscillations which are
331 different for each experiment, but the strong attachment ensures that the number and position of the
332 bacteria is well-preserved throughout each single analysis.

333 As detailed in previous works, to generate dose-dependence curves we compared several parallel
334 experiments in which the bacteria were exposed to different concentrations of antibiotic drugs. To
335 obtain these graphs we focused on the relative reduction of the fluctuations compared to the
336 maximum variance measured before the exposure to the chosen drug concentration. In this way we
337 were able to define a comparative measure of the bacterial response and to compare and average the
338 many experiments we have performed. Each experiment was performed at least in triplicate, lasted
339 at least 2 hours and comprised three steps: i) preparation of viable bacteria in medium (BCG or *M.*
340 *abscessus* in MGIT medium); ii) exposure to the desired drug concentration (INH, RIF or AK); iii)
341 exposure to a high bactericidal drug concentration.(31) The concentration dependence curve was
342 then fitted with a sigmoid curve interpolation, bearing a similar information content of a
343 conventional antibiogram. By performing a linear fitting of the central part of the sigmoid, we
344 calculated two concentration values which can be associated to the minimum inhibitory
345 concentration (MIC - the drug concentration that inhibits visible bacterial growth) and the minimum
346 bactericidal concentration (MBC - the concentration that ensures the death of 99.9% of the
347 bacteria)(31). New AST assays, intended as substitute of conventional microbiological procedures
348 should provide these two concentrations, and this is one of the main advantages of phenotypic
349 assays compared to faster molecular counterparts. Indeed, just as for the conventional values, at
350 drug concentrations below the NM-MIC, the fluctuations of the cantilever are largely unaffected,
351 while at values higher than the NM-MBC the movements are largely reduced.

352

353 **Statistical analysis**

354 The nanomotion data is presented as acquired, with a simple linear fit to remove any long-term drift
355 from the traces. The variance calculations are presented as histograms \pm SD calculated on the
356 corresponding fluctuations over the corresponding raw data, but the trends are indicative of at least
357 three independent sample preparations.

358 Each datapoint of the dose-dependence graphs was obtained from minimally three independent
359 experiments and the graphs were drawn following the procedures detailed elsewhere.(31) The error
360 bars represent the variability of the different experiments performed at each concentration.

361

362 **Acknowledgments**

363 The authors thanks A. Kalauzi and K. Radotic from the Center for Multidisciplinary Studies,
364 Laboratory of Biophysics, University of Belgrade, for their help in for the nanomotion data
365 processing.

366

367 **Funding**

368 GL, SD and MG were funded by the Consiglio Nazionale delle Ricerche, Short term mobility
369 program n. CUP B53C17001680005.

370 SK, GD and LV were funded by the Swiss National Grants 200021-144321 and 407240_167137,
371 the Gebert Rűf Stiftung GRS-024/14 and NASA NNH16ZDA001N-CLDTCH.

372 No funding bodies had any role in study design, data collection and analysis, decision to publish, or
373 preparation of the manuscript.

374

375 **Data availability**

376 All the presented data is available upon reasonable request. Figures 1, 2, 3, 5, 6 and 7 present raw
377 data.

378 All data collection and analysis were performed using custom Labview code, which is freely
379 available upon reasonable request.

380

381 **Author contributions**

382 GL, AM and LV performed the nanomotion experiments; SK and GD provided the nanomotion
383 sensor infrastructure; GL, SK and GD developed and optimized the methodology; GL and LV
384 developed the software; AM and LF provided and characterized the BCG; KB and RAF provided
385 and characterized the *M. abscessus*; GL, LV, SD and MG performed the data analysis; GL, LV,
386 AM, SD and MG wrote the manuscript; all authors read and commented on the manuscript.

387

388 **Transparency declaration**

389 The authors declare no competing interests

390

391

References

- 392 1. Franck J, Arafah K, Elayed M, Bonnel D, Vergara D, Jacquet A, Vinatier D, Wisztorski M,
393 Day R, Fournier I, Salzet M. 2009. MALDI Imaging Mass Spectrometry. *Molecular &*
394 *Cellular Proteomics* 8:2023-2033.
- 395 2. Fournier P-E, Drancourt M, Colson P, Rolain J-M, Scola BL, Raoult D. 2013. Modern
396 clinical microbiology: new challenges and solutions. *Nat Rev Micro* 11:574-585.
- 397 3. Goff DA, Jankowski C, Tenover FC. 2012. Using Rapid Diagnostic Tests to Optimize
398 Antimicrobial Selection in Antimicrobial Stewardship Programs. *Pharmacotherapy* 32:677-
399 687.
- 400 4. Steward CD, Raney PM, Morrell AK, Williams PP, McDougal LK, Jevitt L, McGowan JE,
401 Jr., Tenover FC. 2005. Testing for induction of clindamycin resistance in erythromycin-
402 resistant isolates of *Staphylococcus aureus*. *J Clin Microbiol* 43:1716-21.
- 403 5. Horvat RT. 2010. Review of Antibiogram Preparation and Susceptibility Testing Systems.
404 *Hospital Pharmacy* 45:S6-S9.
- 405 6. Cosgrove SE. 2006. The relationship between antimicrobial resistance and patient outcomes:
406 mortality, length of hospital stay, and health care costs. *Clinical Infectious Diseases* 42:S82-
407 S89.
- 408 7. Seale AC, Gordon NC, Islam J, Peacock SJ, Scott JAG. 2017. AMR Surveillance in low and
409 middle-income settings - A roadmap for participation in the Global Antimicrobial
410 Surveillance System (GLASS). *Wellcome Open Research* 2:92.
- 411 8. Safavieh M, Pandya HJ, Venkataraman M, Thirumalaraju P, Kanakasabapathy MK, Singh
412 A, Prabhakar D, Chug MK, Shafiee H. 2017. Rapid Real-Time Antimicrobial Susceptibility
413 Testing with Electrical Sensing on Plastic Microchips with Printed Electrodes. *ACS Applied*
414 *Materials & Interfaces* 9:12832-12840.
- 415 9. Syal K, Shen S, Yang Y, Wang S, Haydel SE, Tao N. 2017. Rapid Antibiotic Susceptibility
416 Testing of Uropathogenic *E. coli* by Tracking Submicron Scale Motion of Single Bacterial
417 Cells. *ACS Sensors* 2:1231-1239.
- 418 10. Liu C-Y, Han Y-Y, Shih P-H, Lian W-N, Wang H-H, Lin C-H, Hsueh P-R, Wang J-K,
419 Wang Y-L. 2016. Rapid bacterial antibiotic susceptibility test based on simple surface-
420 enhanced Raman spectroscopic biomarkers. *Scientific Reports* 6:23375.
- 421 11. Syal K, Iriya R, Yang Y, Yu H, Wang S, Haydel SE, Chen H-Y, Tao N. 2016.
422 Antimicrobial Susceptibility Test with Plasmonic Imaging and Tracking of Single Bacterial
423 Motions on Nanometer Scale. *ACS Nano* 10:845-852.
- 424 12. Schubert S, Kostrzewa M. 2015. Chapter 14 - MALDI-TOF Mass Spectrometry in the
425 Clinical Microbiology Laboratory; Beyond Identification, p 501-524. *In* Andrew S, Yi-Wei
426 T (ed), *Methods in Microbiology*, vol Volume 42. Academic Press.
- 427 13. Pulido MR, Garcia-Quintanilla M, Martin-Pena R, Cisneros JM, McConnell MJ. 2013.
428 Progress on the development of rapid methods for antimicrobial susceptibility testing. *J*
429 *Antimicrob Chemother* 68:2710-7.
- 430 14. Didelot X, Bowden R, Wilson DJ, Peto TE, Crook DW. 2012. Transforming clinical
431 microbiology with bacterial genome sequencing. *Nat Rev Genet* 13:601-12.
- 432 15. Dinarelli S, Girasole M, Kasas S, Longo G. 2017. Nanotools and molecular techniques to
433 rapidly identify and fight bacterial infections. *J Microbiol Methods* 138:72-81.
- 434 16. Mokrousov I, Chernyaeva E, Vyazovaya A, Sinkov V, Zhuravlev V, Narvskaya O. 2016.
435 Next-Generation Sequencing of *Mycobacterium tuberculosis*. *Emerging infectious diseases*
436 22:1127-1129.
- 437 17. Mittman SA, Huard RC, Della-Latta P, Whittier S. 2009. Comparison of BD Phoenix to
438 Vitek 2, MicroScan MICroSTREP, and Etest for Antimicrobial Susceptibility Testing of
439 *Streptococcus pneumoniae*. *Journal of Clinical Microbiology* 47:3557-3561.

- 440 18. Rhoads S, Marinelli L, Imperatrice CA, Nachamkin I. 1995. Comparison of MicroScan
441 WalkAway system and Vitek system for identification of gram-negative bacteria. *J Clin*
442 *Microbiol* 33:3044-6.
- 443 19. Boisen A, Dohn S, Keller SS, Schmid S, Tenje M. 2011. Cantilever-like micromechanical
444 sensors. *Reports on Progress in Physics* 74:036101.
- 445 20. Domínguez CM, Kosaka PM, Sotillo A, Mingorance J, Tamayo J, Calleja M. 2015. Label-
446 Free DNA-Based Detection of Mycobacterium tuberculosis and Rifampicin Resistance
447 through Hydration Induced Stress in Microcantilevers. *Analytical Chemistry* 87:1494-1498.
- 448 21. Etayash H, Khan MF, Kaur K, Thundat T. 2016. Microfluidic cantilever detects bacteria and
449 measures their susceptibility to antibiotics in small confined volumes. *Nature*
450 *Communications* 7:12947.
- 451 22. Pelling AE, Sehati S, Gralla EB, Valentine JS, Gimzewski JK. 2004. Local nanomechanical
452 motion of the cell wall of *Saccharomyces cerevisiae*. *Science* 305:1147-1150.
- 453 23. Radmacher M, Fritz M, Hansma HG, Hansma PK. 1994. Direct Observation of Enzyme-
454 Activity with the Atomic-Force Microscope. *Science* 265:1577-1579.
- 455 24. Schneider SW, Egan ME, Jena BP, Guggino WB, Oberleithner H, Geibel JP. 1999.
456 Continuous detection of extracellular ATP on living cells by using atomic force microscopy.
457 *PNAS* 96:12180-12185.
- 458 25. Braun T, Ghatkesar MK, Backmann N, Grange W, Boulanger P, Letellier L, Lang H-P,
459 Bietsch A, Gerber C, Hegner M. 2009. Quantitative time-resolved measurement of
460 membrane protein-ligand interactions using microcantilever array sensors. *Nature*
461 *Nanotechnology* 4:179-185.
- 462 26. Ndieyira JW, Watari M, Barrera AD, Zhou D, Vogtli M, Batchelor M, Cooper MA, Strunz
463 T, Horton MA, Abell C, Rayment T, Aepli G, McKendry RA. 2008. Nanomechanical
464 detection of antibiotic mucopeptide binding in a model for superbug drug resistance. *Nature*
465 *Nanotechnology* 3:691-696.
- 466 27. Berger R, Delamarche E, Lang HP, Gerber C, Gimzewski JK, Meyer E, Guntherodt HJ.
467 1997. Surface stress in the self-assembly of alkanethiols on gold. *Science* 276:2021-2024.
- 468 28. Burg TP, Godin M, Knudsen SM, Shen W, Carlson G, Foster JS, Babcock K, Manalis SR.
469 2007. Weighing of biomolecules, single cells and single nanoparticles in fluid. *Nature*
470 446:1066-1069.
- 471 29. Park K, Millet LJ, Kim N, Li H, Jin X, Popescu G, Aluru NR, Hsia KJ, Bashir R. 2010.
472 Measurement of adherent cell mass and growth. *Proceedings of the National Academy of*
473 *Sciences* 107:20691-20696.
- 474 30. Kasas S, Longo G, Alonso-Sarduy L, Dietler G. 2011. Nanoscale Motion Detector. Patent
475 Switzerland patent PCT/IB2011054553.
- 476 31. Longo G, Alonso Sarduy L, Rio LM, Bizzini A, Trampuz A, Notz J, Dietler G, Kasas S.
477 2013. Rapid detection of bacterial resistance to antibiotics using AFM cantilevers as
478 nanomechanical sensors. *Nat Nano* 8:522-526.
- 479 32. Kasas S, Ruggeri FS, Benadiba C, Maillard C, Stupar P, Tournu H, Dietler G, Longo G.
480 2015. Detecting nanoscale vibrations as signature of life. *Proceedings of the National*
481 *Academy of Sciences* 112:378-381.
- 482 33. Alonso-Sarduy L, De Los Rios P, Benedetti F, Vobornik D, Dietler G, Kasas S, Longo G.
483 2014. Real-Time Monitoring of Protein Conformational Changes Using a Nano-Mechanical
484 Sensor. *PLoS ONE* 9:e103674.
- 485 34. Ruggeri FS, Mahul-Mellier A-L, Kasas S, Lashuel HA, Longo G, Dietler G. 2017. Amyloid
486 single-cell cytotoxicity assays by nanomotion detection. *Cell Death Discov* 3:17053.
- 487 35. Lissandrello C, Inci F, Francom M, Paul MR, Demirci U, Ekinici KL. 2014.
488 Nanomechanical motion of *Escherichia coli* adhered to a surface. *Appl Phys Lett*
489 105:113701.

- 490 36. Wu S, Liu X, Zhou X, Liang XM, Gao D, Liu H, Zhao G, Zhang Q, Wu X. 2016.
491 Quantification of cell viability and rapid screening anti-cancer drug utilizing
492 nanomechanical fluctuation. *Biosensors and Bioelectronics* 77:164-173.
- 493 37. Yang F, Riedel R, Del Pino P, Pelaz B, Said AH, Soliman M, Pinnapireddy SR, Feliu N,
494 Parak WJ, Bakowsky U, Hampp N. 2017. Real-time, label-free monitoring of cell viability
495 based on cell adhesion measurements with an atomic force microscope. *J*
496 *Nanobiotechnology* 15:23.
- 497 38. Ines VM, Petar S, Wojciech C, Massimiliano B, Giovanni D, Laura A, Elena VM, Osvaldo
498 Y, Sandor K. 2018. Nanomotion Detection Method for Testing Antibiotic Resistance and
499 Susceptibility of Slow-Growing Bacteria. *Small* 14:1702671.
- 500 39. Stupar P, Opota O, Longo G, Prod'hom G, Dietler G, Greub G, Kasas S. 2017.
501 Nanomechanical sensor applied to blood culture pellets: a fast approach to determine the
502 antibiotic susceptibility against agents of bloodstream infections. *Clin Microbiol Infect*
503 23:400-405.
- 504 40. Beaussart A, El-Kirat-Chatel S, Herman P, Alsteens D, Mahillon J, Hols P, Dufrene YF.
505 2013. Single-cell force spectroscopy of probiotic bacteria. *Biophys J* 104:1886-92.
- 506 41. Tortoli E. 2014. Microbiological features and clinical relevance of new species of the genus
507 *Mycobacterium*. *Clin Microbiol Rev* 27:727-52.
- 508 42. Zumla AI, Gillespie SH, Hoelscher M, Philips PP, Cole ST, Abubakar I, McHugh TD,
509 Schito M, Maeurer M, Nunn AJ. 2014. New antituberculosis drugs, regimens, and adjunct
510 therapies: needs, advances, and future prospects. *The Lancet infectious diseases* 14:327-340.
- 511 43. Calvori C, Frontali L, Leoni L, Tecce G. 1965. Effect of Rifamycin on Protein Synthesis.
512 *Nature* 207:417.
- 513 44. Marianelli C, Armas F, Boniotti MB, Mazzone P, Pacciarini ML, Di Marco Lo Presti V.
514 2015. Multiple drug-susceptibility screening in *Mycobacterium bovis*: new nucleotide
515 polymorphisms in the embB gene among ethambutol susceptible strains. *International*
516 *Journal of Infectious Diseases* 33:39-44.
- 517 45. Kolibab K, Derrick SC, Morris SL. 2011. Sensitivity to isoniazid of *Mycobacterium bovis*
518 BCG strains and BCG disseminated disease isolates. *Journal of clinical microbiology*
519 49:2380-2381.
- 520 46. Rastogi N, Goh K, Berchel M, Bryskier A. 2000. Activity of rifapentine and its metabolite
521 25-O-desacetyl-rifapentine compared with rifampicin and rifabutin against *Mycobacterium*
522 *tuberculosis*, *Mycobacterium africanum*, *Mycobacterium bovis* and *M. bovis* BCG. *Journal*
523 *of Antimicrobial Chemotherapy* 46:565-570.
- 524 47. Aon MA, Roussel MR, Cortassa S, O'Rourke B, Murray DB, Beckmann M, Lloyd D. 2008.
525 The Scale-Free Dynamics of Eukaryotic Cells. *PLOS ONE* 3:e3624.
- 526 48. Lloyd D, Cortassa S, O'Rourke B, Aon MA. 2012. What yeast and cardiomyocytes share:
527 ultradian oscillatory redox mechanisms of cellular coherence and survival. *Integr Biol*
528 (Camb) 4:65-74.
- 529 49. Kruse K, Julicher F. 2005. Oscillations in cell biology. *Curr Opin Cell Biol* 17:20-6.
- 530 50. Schembri MA, Christiansen G, Klemm P. 2001. FimH-mediated autoaggregation of
531 *Escherichia coli*. *Mol Microbiol* 41:1419-30.
- 532 51. Maurer FP, Bruderer VL, Castelberg C, Ritter C, Scherbakov D, Bloemberg GV, Bottger
533 EC. 2015. Aminoglycoside-modifying enzymes determine the innate susceptibility to
534 aminoglycoside antibiotics in rapidly growing mycobacteria. *J Antimicrob Chemother*
535 70:1412-9.
- 536 52. Pryjma M, Burian J, Kuchinski K, Thompson CJ. 2017. Antagonism between Front-Line
537 Antibiotics Clarithromycin and Amikacin in the Treatment of *Mycobacterium abscessus*
538 Infections Is Mediated by the whiB7 Gene. *Antimicrob Agents Chemother* 61.

- 539 53. Ibrahim EH, Sherman G, Ward S, Fraser VJ, Kollef MH. 2000. The influence of inadequate
540 antimicrobial treatment of bloodstream infections on patient outcomes in the ICU setting.
541 *Chest* 118:146-155.
- 542 54. Premanandh J, Samara BS, Mazen AN. 2015. Race Against Antimicrobial Resistance
543 Requires Coordinated Action – An Overview. *Frontiers in Microbiology* 6:1536.
- 544 55. Imperi F, Leoni L, Visca P. 2014. Antivirulence activity of azithromycin in *Pseudomonas*
545 *aeruginosa*. *Frontiers in Microbiology* 5.
- 546 56. Rampioni G, Visca P, Leoni L, Imperi F. 2017. Drug repurposing for antivirulence therapy
547 against opportunistic bacterial pathogens. *Emerging Topics in Life Sciences*
548 doi:10.1042/etls20160018.
- 549 57. Formentin P, Catalan U, Pol L, Fernandez-Castillejo S, Sola R, Marsal LF. 2018. Collagen
550 and fibronectin surface modification of nanoporous anodic alumina and macroporous silicon
551 for endothelial cell cultures. *J Biol Eng* 12:21.
- 552 58. Kim YH, Baek NS, Han YH, Chung MA, Jung SD. 2011. Enhancement of neuronal cell
553 adhesion by covalent binding of poly-D-lysine. *J Neurosci Methods* 202:38-44.
- 554 59. Lupoli F, Vannocci T, Longo G, Niccolai N, Pastore A. 2018. The role of oxidative stress in
555 Friedreich's ataxia. *FEBS Letters* 592:718-727.
- 556 60. Dinarelli S, Girasole M, Longo G. 2018. FC_analysis: a tool for investigating atomic force
557 microscopy maps of force curves. *BMC Bioinformatics* 19:258.
- 558 61. Aghayee S, Benadiba C, Notz J, Kasas S, Dietler G, Longo G. 2013. Combination of
559 fluorescence microscopy and nanomotion detection to characterize bacteria. *Journal of*
560 *Molecular Recognition* 26:590-595.
- 561 62. Kasas S, Radotic K, Longo G, Saha B, Alonso-Sarduy L, Dietler G, Roduit C. 2013. A
562 universal fluid cell for the imaging of biological specimens in the atomic force microscope.
563 *Microsc Res Tech* 76:357-363.

564

565

566 **Figure captions**

567

568 **Figure 1. Control experiments involving BCG and *M. abscessus*.** Typical data patterns
569 (performed minimally in triplicate) of BCG (panel a) and *M. abscessus* (panel b) in MGIT medium.
570 The fluctuations are present for more than 200 minutes.

571

572 **Figure 2. Nanomotion experiments on BCG exposed to an over-MIC dose of INH.** Top panel.
573 Typical 10 minutes segments of the sensor's fluctuations: before the exposure to INH (left);
574 immediately after the exposure to INH at 2 $\mu\text{g/ml}$ (center); 20 minutes after the exposure to INH,
575 when the movement reduction has stabilized. Lower panel. Histogram of the corresponding
576 variance of the fluctuations. The graph is representative of minimally 5 independent experiments
577 which produced similar results. The error bars in the variance histogram represent \pm SD of the
578 corresponding fluctuations over the shown 10-minute time-period.

579

580 **Figure 3. Nanomotion experiments on BCG exposed to an over-MIC dose of RIF.** Top panel.
581 Typical 20 minutes segments of the sensor's fluctuations: before the exposure to RIF (left);
582 immediately after the exposure to RIF at 0.7 $\mu\text{g/ml}$ (center); 80 minutes after the exposure to RIF,
583 when the movement reduction has stabilized. Lower panel. Histogram of the corresponding
584 variance of the fluctuations. The graph is representative of 3 independent experiments which
585 produced similar results. The error bars in the variance histogram represent \pm SD of the
586 corresponding fluctuations over the shown 20-minute time-period.

587

588 **Figure 4. Dose dependence experiments.** Panel a. Normalized variance calculated from the
589 deflections collected by exposing the BCG to different INH concentrations. Panel b. Normalized
590 variance calculated from the deflections collected by exposing the BCG to different RIF
591 concentrations. Panel c. Normalized variance calculated from the deflections collected by exposing
592 the *M. abscessus* to different AK concentrations. The concentration values can be well fitted with a
593 sigmoid function, which is comparable with the antibiogram plots, obtained using conventional
594 microbiological techniques. The MIC and the MBC of towards the bacterial species can be obtained
595 by calculating the tangent of the sigmoid fit at half height (black dashed line). Each data-point
596 represents the average of a minimum of 3 independent experiments performed using the same drug
597 concentration. The error bars represent the variability of the different experiments performed at the
598 same concentration. In each graph, the experiments involving sub-MIC drug concentrations are
599 represented as a single data-point, which summarizes all these experiments.

600

601 **Figure 5. Nanomotion experiments on BCG exposed to a sub-MIC dose of INH and RIF.** Panel
602 a: Top panel. Typical 20 minutes segments of the sensor's fluctuations: before the exposure to INH
603 (left); immediately after the exposure to INH at 0.025 $\mu\text{g/ml}$ (center); 140 minutes after the
604 exposure to INH, when the movement has stabilized. Lower panel. Histogram of the corresponding
605 variance of the fluctuations. Panel b: Top panel. Typical 20 minutes segments of the sensor's
606 fluctuations: before the exposure to RIF (left); immediately after the exposure to RIF at 0.07 $\mu\text{g/ml}$
607 (centre); 95 minutes after the exposure to RIF, when the movement has stabilized. Lower panel.
608 Histogram of the corresponding variance of the fluctuations. Each graph is representative of
609 minimally 3 independent experiments which produced similar results. The error bars in the variance
610 histogram represent \pm SD of the corresponding fluctuations over the shown 20-minute time-period.

611 **Figure 6. Time-resolved analysis of the BCG response to INH.** Typical data pattern of the
612 response of BCG to a bactericidal dose of INH (1 $\mu\text{g}/\text{ml}$). Over a 140-minute period, the
613 fluctuations increase and decrease in amplitude, highlighting the bacterial response to the antibiotic
614 pressure. The graph is representative of 3 independent experiments in which this feature was
615 evidenced.

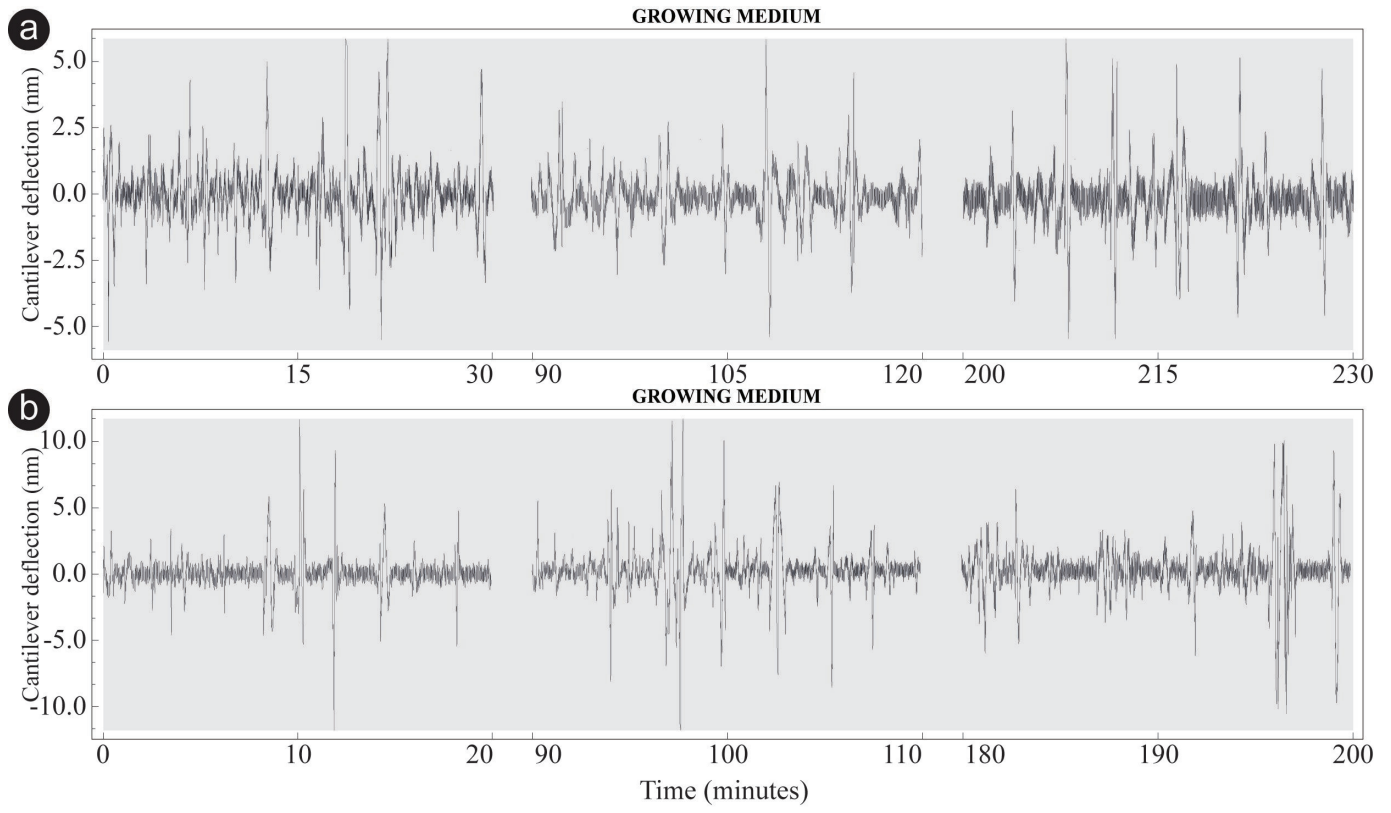
616

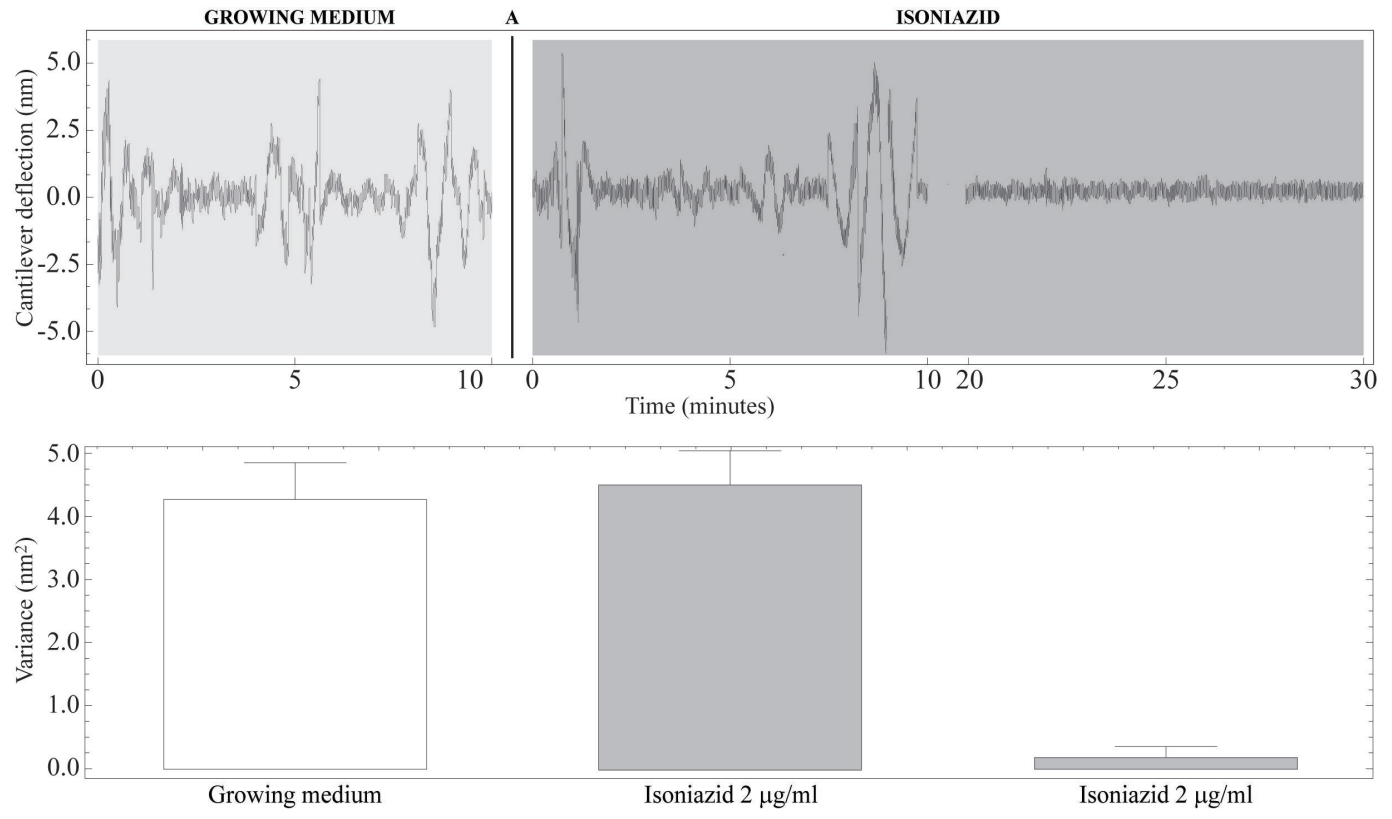
617 **Figure 7. Nanomotion experiments on *M. abscessus* exposed to AK.** Panel a: Top panel. Typical
618 20 minutes segments of the sensor's fluctuations exposed to an over-MIC dose of AK: before the
619 exposure to AK (left); immediately after the exposure to AK at 10 $\mu\text{g}/\text{ml}$ (center); 50 minutes after
620 the exposure to AK, when the movement has stabilized. Lower panel. Histogram of the
621 corresponding variance of the fluctuations. Panel b: Top panel. Typical 20 minutes segments of the
622 sensor's fluctuations exposed to a sub-MIC dose of AK: before the exposure to AK (left); 30
623 minutes after the exposure to AK at 1 $\mu\text{g}/\text{ml}$ (center); 90 minutes after the exposure to AK, when
624 the movement has recovered and stabilized. Lower panel. Histogram of the corresponding variance
625 of the fluctuations. Each graph is representative of at least 3 independent experiments which
626 produced similar results. The error bars in the variance histogram represent \pm SD of the
627 corresponding fluctuations over the shown 20-minute time-period.

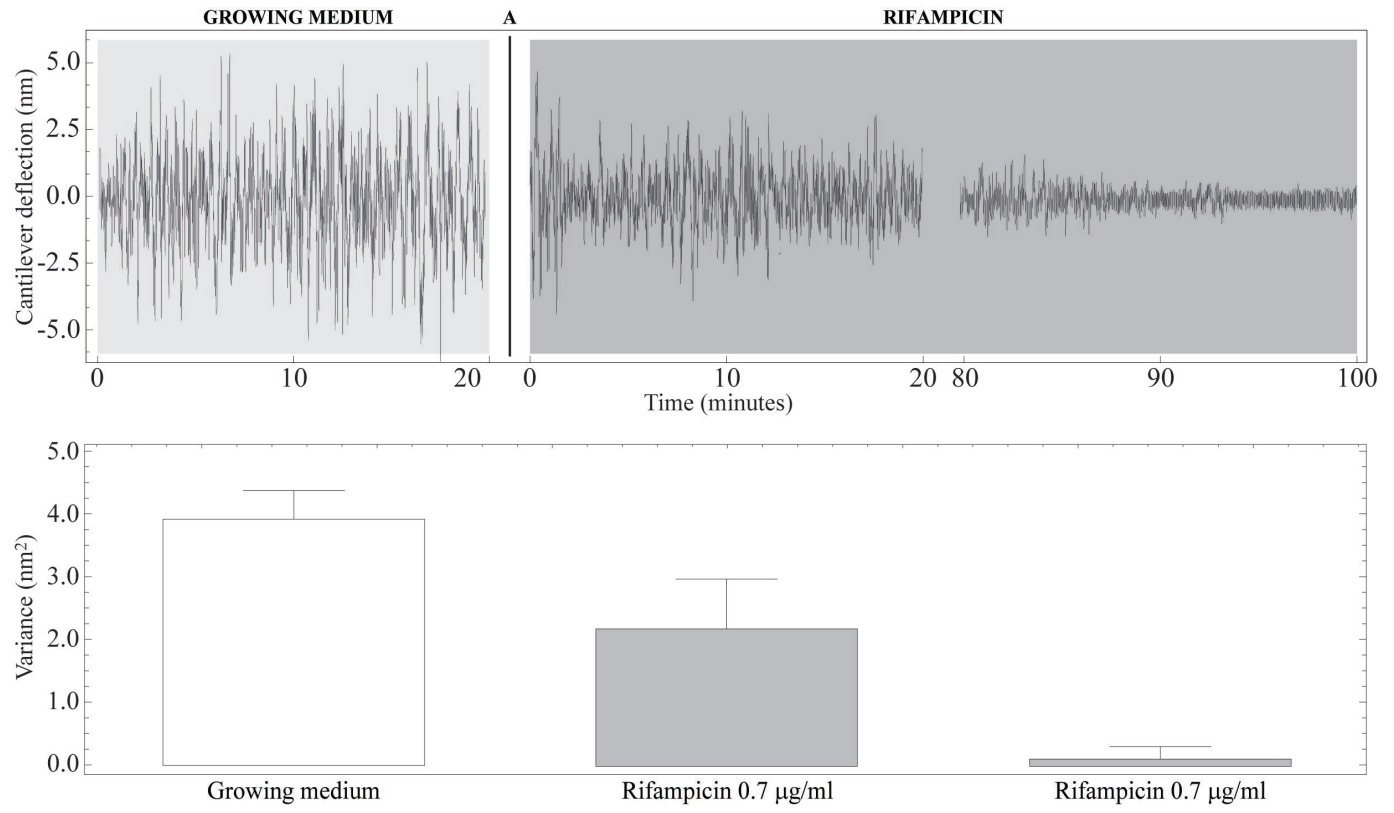
628

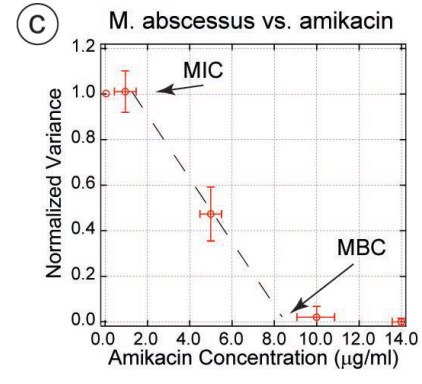
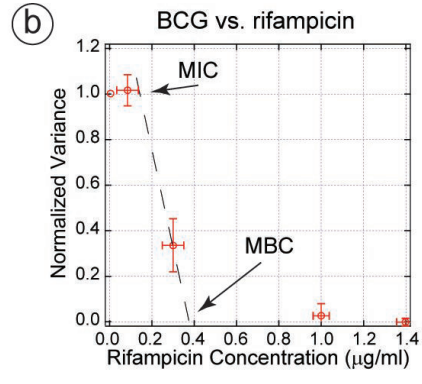
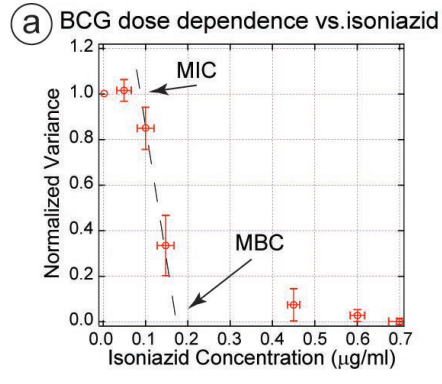
629 **Figure 8. Optical images of bacteria-bearing sensors.** Typical optical images of rectangular (left
630 panels) and triangular sensors (right panels) bearing BCG (panel a) and *M. abscessus* (panel b). The
631 optical images show the BCG clumping. The scale bars indicate 50 μm .

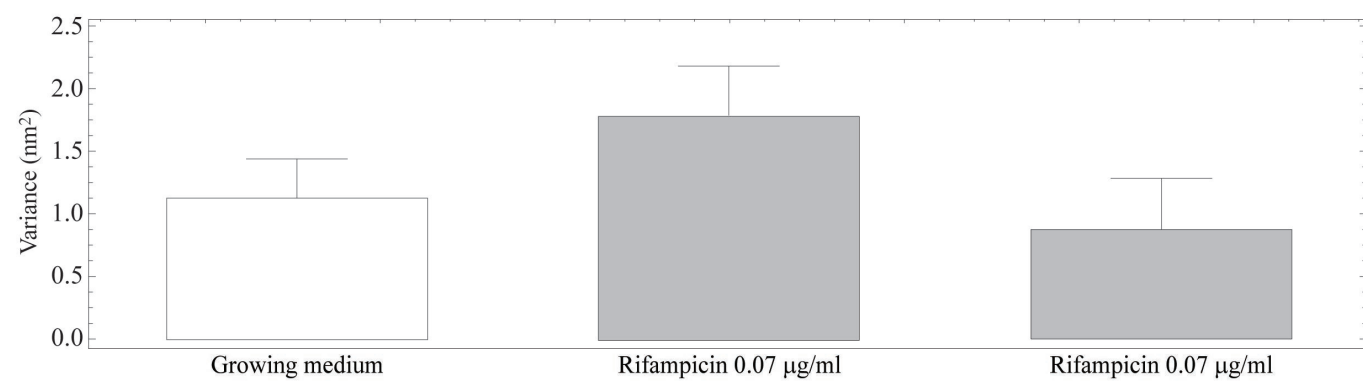
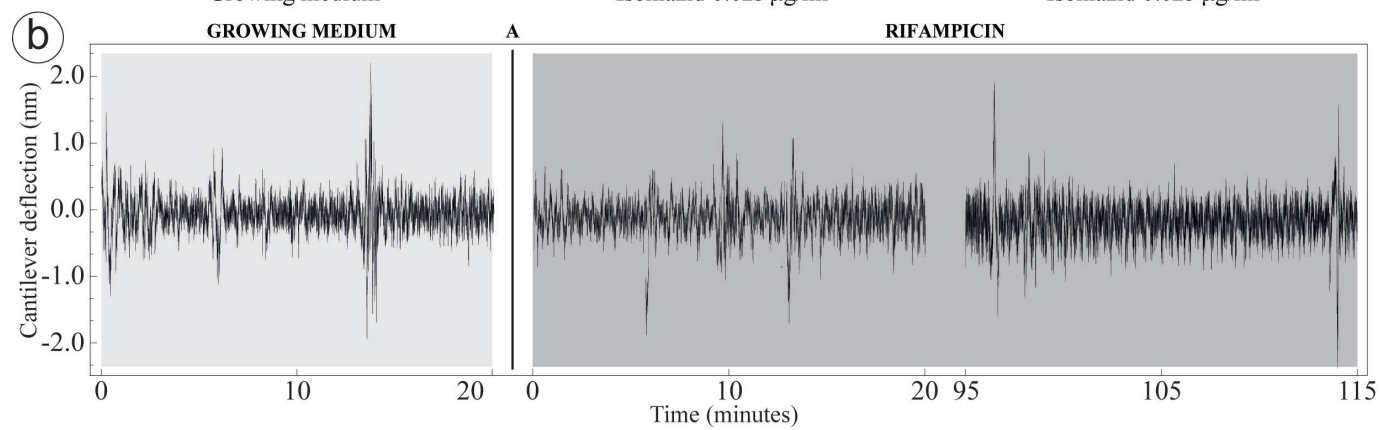
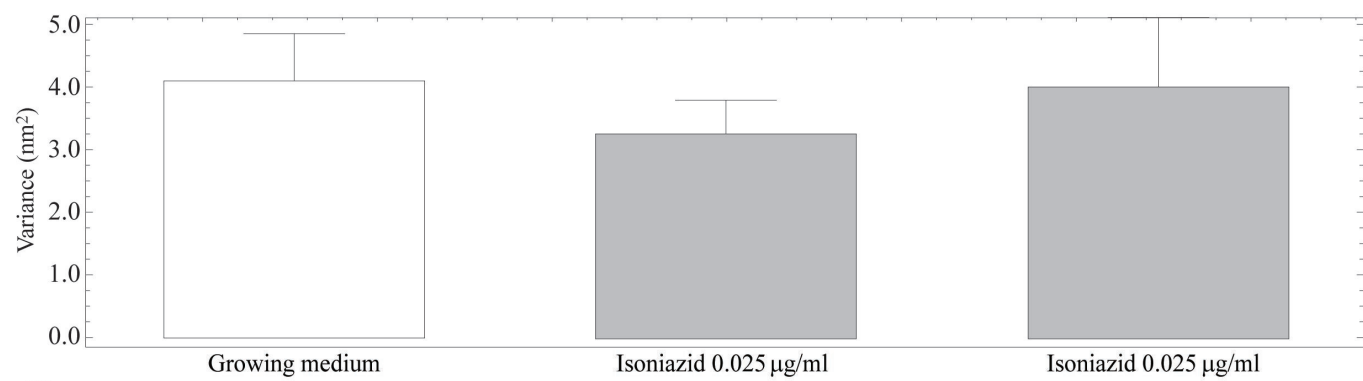
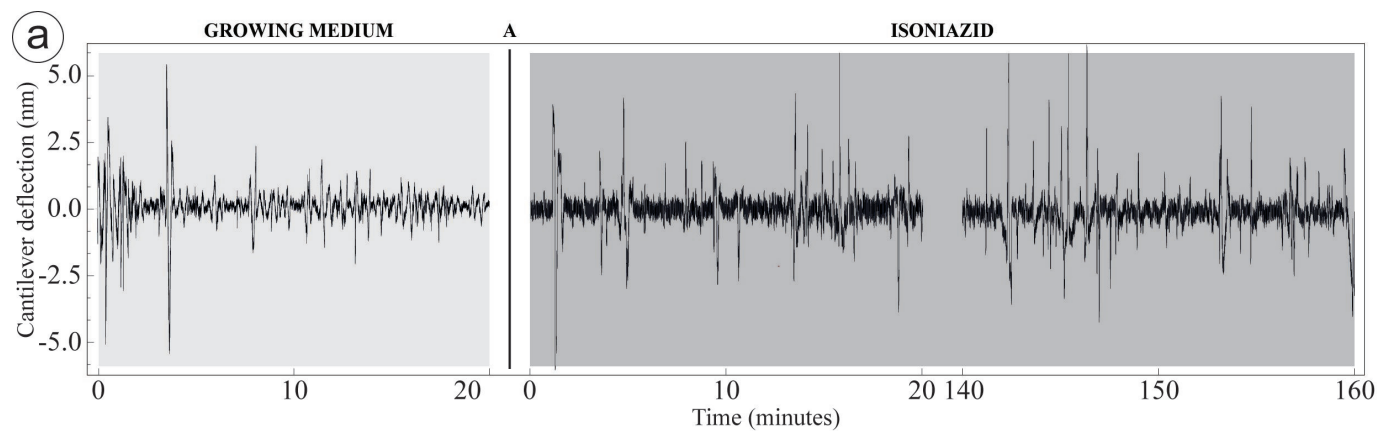
632

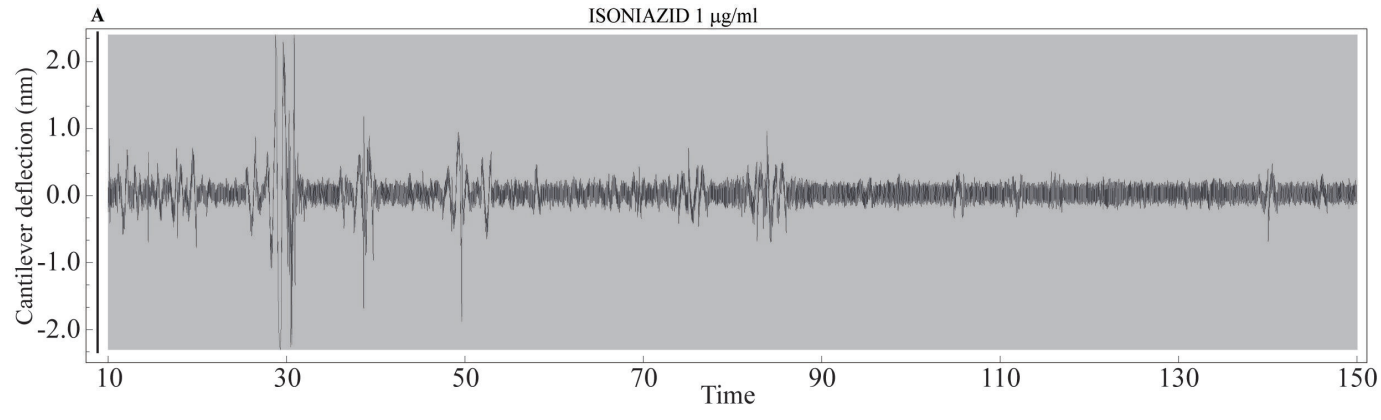


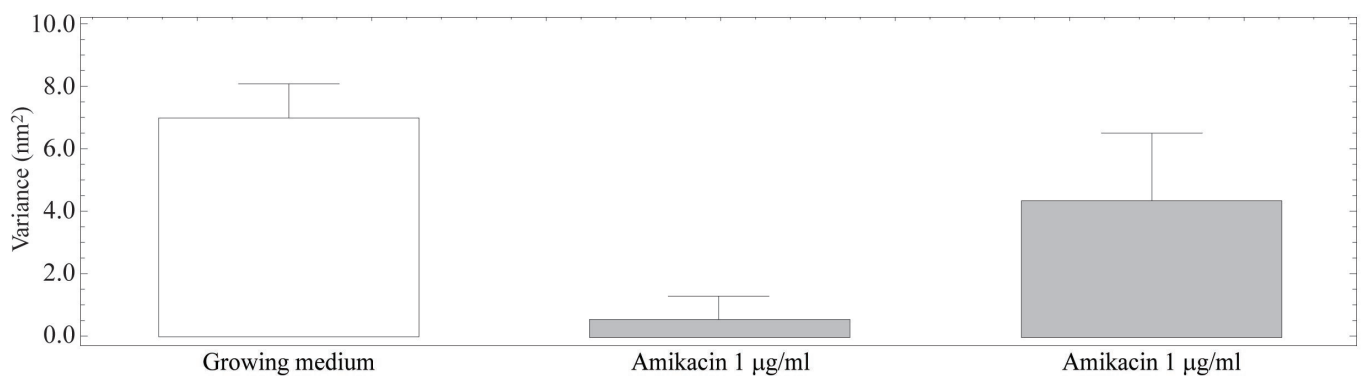
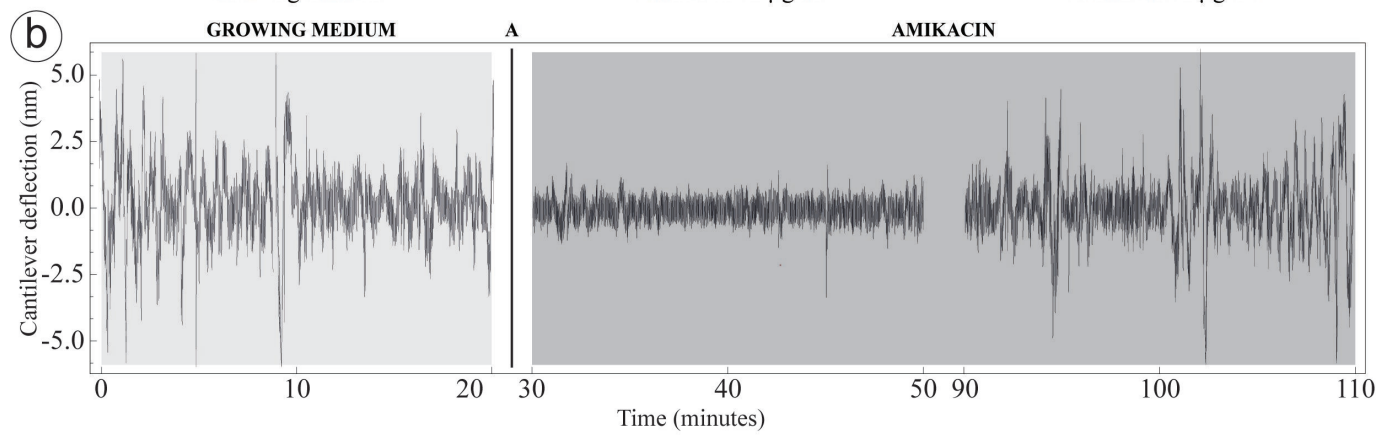
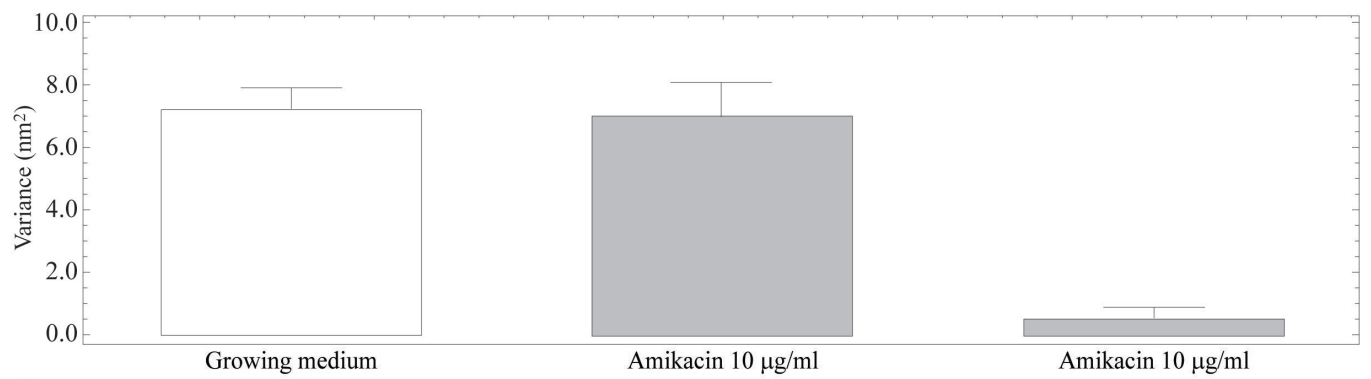
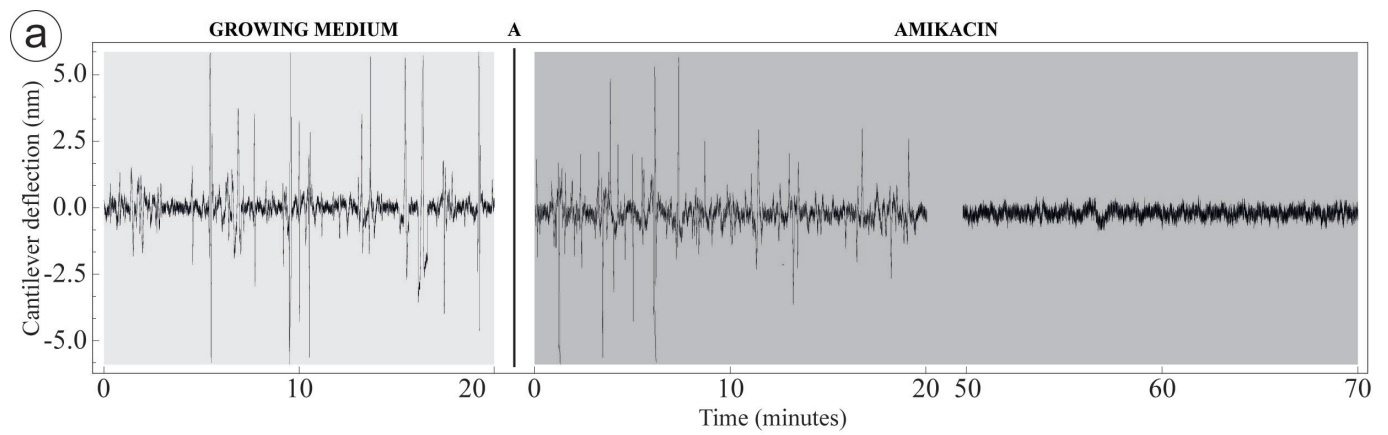




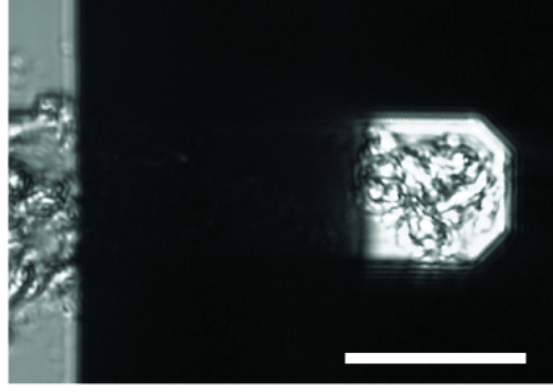








a



b

